No. 6

Available online at www.sciencedirect.com
SCIENCE DIRECT®
ELSEVIER
Journal of Non-Crystalline Solids 315 (2003) 276–287
JOURNAL OF NON-CRYSTALLINE SOLIDS
www.elsevier.com/locate/jnoncrysol

Epoxy based coatings on glass: strengthening mechanisms

R.J. Hand *, B. Ellis, B.R. Whittle, F.H. Wang [1]

Centre for Glass Research, Department of Engineering Materials, Sir Robert Hadfield Building, University of Sheffield, Mappin Street, Sheffield S1 3JD, UK

Received 9 October 2001; received in revised form 22 May 2002

Abstract

Glass may be strengthened by epoxy coatings although the strengthening mechanisms remain unclear. Possible strengthening mechanisms are reviewed and are used to analyse strength data for both a solvent based and a water based coating system. The coatings either fill (solvent based coatings), or partially fill (water based coatings) surface cracks and it is shown that closure stresses arising from the thermal expansion mismatch of the coating within these cracks can account for the observed degrees of strengthening. It is also demonstrated that other suggested mechanisms such as flaw healing cannot fully account for the observed degree of strengthening.

PACS: 62.20.Mk; 68.35.Gy

1. Introduction

It is well established that glass may be strengthened by use of surface coatings (see, for example, [1–8]). A number of suggestions have been made as to how these coatings actually strengthen glass ranging from residual stresses to flaw healing processes. However, despite a number of publications in this area, questions remain concerning the strengthening process and it is the intention of the current work to review the suggested mechanisms with particular reference to both a solvent based and a water based epoxy coating system previously described [4–7].

2. Background

Glass fails to achieve its theoretical strength because of the presence of small surface defects. One way to overcome pre-existing defects (and possibly to prevent the formation of further defects) is to coat the surface. A number of coating systems have been developed for this purpose including sol–gel based systems [1,2] and epoxy coating systems [4–7]. In both cases, there is evidence that the flaws are, at least partially, filled by the coating. Most of this evidence has been obtained by studying the coating of glass containing large Vicker's indentations which are used as model 'uniform' defects to give a controlled

* Corresponding author. Tel.: +44-114 222 5465; fax: +44-114 222 5943.
E-mail address: r.hand@sheffield.ac.uk (R.J. Hand).
[1] Present address: Technical Services, ACI Packaging, 310-324 Ferntree Gully Road, North Clayton, Vic. 3168, Australia.

0022-3093/03/$ - see front matter
PII: S0022-3093(02)01611-3

narrow distribution of strengths. However, despite the evidence that flaw filling occurs, it is much less clear how filling a crack with material that is different from and, in some cases, has a significantly lower Young's modulus than, the surrounding bulk glass, actually leads to this strengthening. Suggestions in the literature include crack length reduction [1,2], Poisson ratio effects [4] and the generation of closure stresses [9].

3. Experimental

Although coatings described in this work were primarily developed to strengthen bottles, it is significantly easier from an experimental point of view to analyse the mechanics of these coatings when they are applied to flat glass. Hence, given that previous work has shown that these coatings do strengthen containers [5], in the current work, we have utilised commercial soda-lime-silicate microscope slides (see Table 1 for analysis). The slides were initially 76 mm long by 26 mm wide and between 1.2 and 1.5 mm thick with polished edges (solvent based coatings work) or 1.1 mm thick with cut edges (water based coatings work). The slides were cut in half to produce samples for coating.

As indicated above, to reduce scatter, controlled defects were introduced into the samples studied in this work using Vicker's indents. Following indentation, the samples were aged in air for 24 h (solvent based coatings work) or 1 week (water based coatings work). Initial work concentrated on quantifying the size and geometry of flaws produced using different loads and the extent of the residual stresses around the flaws. Although allowing the cracks to grow sub-critically after indentation will have relieved some of the residual stresses around the indentation, complete removal of these stresses only occurs on annealing. Therefore, to assess the extent of residual stresses left around the indentation site after the aging process, the mean strength of samples annealed after indentation was compared with that of samples that had not been annealed.

This initial stage of the research was used to determine an appropriate controlled flaw size, and hence, indentation load required to produce the samples for the subsequent coating study. Based on the results of these studies, detailed below, it was decided to use a 10 kg load which resulted in semi-elliptical cracks with a surface length, $2c$ (see Fig. 1(a) and (b)). After the 24 h aging process,

Table 1
Oxide composition of soda-lime-silicate slides used in this work (ICP analysis)

Oxide	Weight %
SiO_2	70.2
Na_2O	14.0
MgO	3.76
CaO	7.08
Al_2O_3	1.38
Others	3.58

(a)

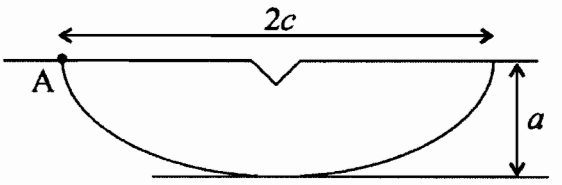

where:
A = crack initiation point
a = crack depth
$2c$ = surface crack length

(b)

Fig. 1. (a) Micrograph of semi-elliptical flaws produced by Vicker's indentation. (b) Schematic diagram of semi-elliptical flaws produced by Vicker's indentation.

$c = 461 \pm 5$ μm, whereas, after the 1 week aging process, $c = 467 \pm 19$ μm. A number of samples were used as controls and were not coated after indentation. The rest of the samples were coated after the indentations had been allowed to age as described.

3.1. Solvent based epoxy/hardener coatings

Solvent based coatings were prepared by mixing 10.5 parts of triethylenetetraamine hardener (HY951, Ciba-Geigy) with 100 parts of a plasticised bisphenol A epoxy resin (MY750, Ciba-Geigy). The mixture was stirred at 25 °C in a water bath for 90 min. The resultant mixture was diluted to 50 wt% with acetone. The slides were cleaned by wiping with tissue paper and then dipped into the coating mixture using a dip coating apparatus; with a dipping angle of 90° and a dipping speed of 1.5 mm s^{-1} a coating thickness of 3 μm was obtained. The resin coating was cured for 24 h at room temperature and post-cured at 100 °C for 1 h. This cure treatment has been shown previously [4] to yield a high strengthening effect. Coatings prepared in this fashion are referred to as EH_{sol} coatings.

Previous work has demonstrated that use of a silane primer prior to dip coating improves the hydrolytic durability of the resultant coating [10]. The silane primer solution was prepared by adding an aminoethyl aminopropyl trimethoxy silane (Z6020, Dow Corning) dropwise to distilled water at room temperature. The final concentration was 1 wt%. The slides were immersed in the solution for 1 h at room temperature and then immersed in distilled water at room temperature for a further hour (designated $S_p/W_{RT}/EH_{sol}$ in the following). This procedure was used as Cheng et al. [11] have shown that water extraction of silane coated glass fibres removes a weak layer of silane gel. In some cases, this treatment was followed by immersion in distilled water at 60 °C for 1 h (designated $S_p/W_{60}/EH_{sol}$ in the following). Silane primed coatings for which the water extraction treatment was not used are designated S_p/EH_{sol}. In all cases, the slides were dried after the priming treatment for 30 min at 120 °C and cooled to room temperature before coating with the 50% acetone solution of resin with hardener as described above. These coatings were again cured for 24 h at room temperature cure followed by a post-cure for 1 h at 100 °C. Some samples were only coated using the silane. These samples were left in air at room temperature for 3 h to ensure gelation and then dried at 60 °C for 1 h. These coatings are referred to as S coatings.

As the use of a silane primer to improve coating durability is a lengthy two step procedure, which would not be commercially viable, additional experiments were conducted with coatings that consisted of mixtures of silane, epoxy resin and hardener. In this case, after the initial pre-reaction of the epoxy/hardener mixture 7.23 wt% of silane was added; this amount of silane has previously been shown to give the maximum strengthening effect [12]. The resultant mixture was diluted to 50 wt% with acetone. To hydrolyse the silane, half the stoichiometric amount of water (1.03 parts per hundred parts resin) was then added. The resulting solution was stirred for 4 h before the slides were dip coated as detailed above. These coatings are referred to as EH_{sol}/S coatings.

3.2. Water based coating systems

Water based coating systems were prepared by mixing 5 g of a proprietory blend of bisphenol A and F epoxy resin (PY340-2, Ciba-Geigy) with 7.5 g of a polyamidoamine hardener (HZ340, Ciba-Geigy). An emulsion was created by slowly adding 50, 75, 100 or 200 g of deionised water, to give solution concentrations of 20, 15, 10 and 5%, respectively, and mixing for 10 min; previous work [5] had shown that the concentration of the coating solution is an important variable in the degree of strengthening that could be achieved with this coating. The slides were again coated by dipping with a dipping angle of 90° and a withdrawal speed of 1.2 mm s^{-1} to give a coating thickness of approximately 10 μm. The coatings were dried at room temperature for 30–90 min and then cured at 220 °C. Coatings prepared in this fashion are referred to as EH_{W_x} coatings where $x = 5$, 10, 15 or 20, the coating solution concentration.

3.3. Mechanical testing

Following these treatments, the failure strengths of the slides were measured using four point bend on a Mayes SM200 universal testing machine. The test-jig was mounted on a flexible support stage to avoid parasitic bending moments due to misalignment of the loading axis. Adhesive tape was placed on the compressive side of the samples, for retension of broken fragments after failure. The loading rate was 2.5 mm min^{-1}. For the solvent based coatings work 6–8 samples were tested for each coating. For the water based coatings work 10 samples were tested for each coating. In both cases, the results are given as mean failure strengths plus/minus one standard deviation.

4. Results and initial analysis

4.1. Generation of controlled flaws

In the initial stage of the work, controlled flaws were produced using indentation loads between 1 and 10 kg (see Table 2). Although most analyses of the cracks produced under a Vicker's indentation assumes that they are semi-circular (see, for example, [13–16]), the flaws obtained throughout this work were approximately semi-elliptical. The flaws studied in the initial stage of the work all had an aspect ratio (a/c value) of 0.6 (Fig. 1(a)). Semi-elliptical flaws have also been observed by other groups (see, for example, [17,18]). The simplest semi-circular analysis for Vicker's indentation flaws suggests that

$$K_{Ic} = \frac{\chi P}{c^{3/2}}, \tag{1}$$

where P is the indentation load; c is the radius of the crack; K_{Ic} is the fracture toughness of the material and χ is an empirically determined constant that is independent of the load and the size. A variety of values have been proposed for χ depending on the model used (see, for example, [19]). Fig. 2 shows a plot of $c^{3/2}$ versus P is a straight line, with a slope of $9.98 \times 10^{-8} \pm 0.12 \times 10^{-8}$ Nm$^{-3/2}$, which indicates that the simple model of Eq. (1) can indeed be used to describe the stress intensity factor around the approximately semi-elliptical indentation flaws obtained in this work. χ was evaluated using Eq. (1) and the slope of the line. Taking K_{Ic} for soda lime glass to be 0.75 MN m$^{3/2}$ [20] the value of χ obtained was 0.075 ± 0.001. This value does not exactly agree with any of the values given in Ponton and Rawlings' review [19], although it is close to the value of 0.0726 given by Marion [21] which is not cited in [19]. Exact agreement would not necessarily be expected because the cracks had grown subcritically by aging which will have affected the value obtained for χ.

Whittle and Hand [22] have shown that the depth of the median/radial crack, a, is limited by the presence of lateral cracks under a Vickers indent. The depth of the lateral crack is determined by the size of the plastic zone [23] which is

Table 2
Mean failure stress and surface crack lengths for indented samples

Indentation load, P (kg)	Failure stress, σ_f (MPa)	Surface crack length, c (μm)
0.5	68 ± 4	62 ± 1
1.0	63 ± 3	88 ± 3
2.0	52 ± 4	150 ± 4
5.0	42 ± 2	283 ± 4
10.0	35 ± 2	461 ± 5
10.0†	30 ± 1	467 ± 19

Sample marked † aged for 1 week all other samples aged for 24 h.

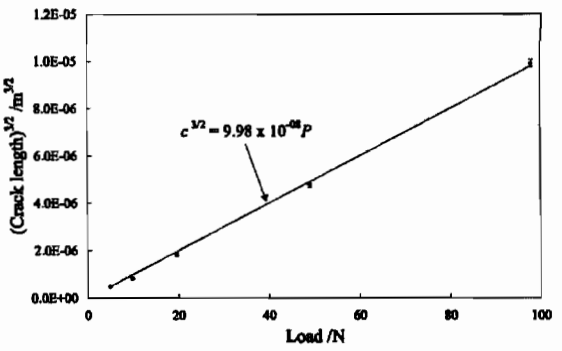

Fig. 2. Plot of (surface crack length)$^{3/2}$ versus indentation load for Vicker's indentation flaws after 24 h aging.

proportional to the square root of the indentation load [24]

$$P \propto a^2. \tag{2}$$

Combining Eqs. (1) and (2) suggests that

$$a = \Omega c^{3/4}, \tag{3}$$

where Ω is a constant, which suggests that the aspect ratio should change with flaw size. Fig. 3 shows a plot of a versus c for a number of samples 1.1 mm thick indented with loads between 1 and 16 kg and annealed immediately after indentation. The solid line is a power law fit to the data giving $a = 2.1453c^{0.7465}$ with an r^2 value of 0.9978 which is essentially the same as Eq. (3). This gives further support to the idea that the median/radial crack depth is indeed limited by the lateral cracks as suggested in [21]. In addition, the results shown in Fig. 3 lend further support to the use of Eq. (1) in evaluating stress intensity factors arising from Vicker's indentation flaws, because, although the results indicate that the crack shape and aspect ratio are not independent of load, the analysis used to arrive at Eq. (3) assumes that Eq. (1) is valid.

Therefore, although the flaws observed in this work are semi-elliptical, it is reasonable to account for the residual stresses around the indent using

$$K_r = \frac{\chi_r P}{c^{3/2}}, \tag{4}$$

where χ_r is a dimensionless number which is determined by the level of residual stress around the indentation crack.

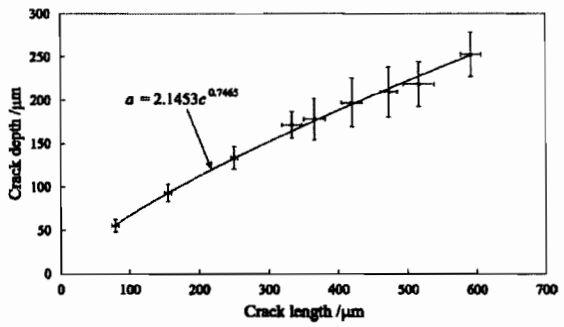

Fig. 3. Plot of crack depth versus surface crack length for Vicker's indentation flaws annealed immediately after indentation.

It should be noted that, although the aspect ratio of the flaws used in the solvent based work was 0.6, the aspect ratio of flaws used in the water based work was 0.42. This discrepancy partly reflects the fact that in the latter case the samples were aged for 1 week rather than 1 day; whilst the surface crack length, c, continues to increase during the aging treatment, the crack depth, a, remains unchanged as growth in this direction is limited by the already formed lateral cracks.

4.2. Residual stresses

The fracture stress of indented glass slides with or without annealing is given as a function of indentation load in Tables 2 and 3. The fracture stress of as received slides was 112 ± 13 MPa. It can be seen from Table 2 that the introduction of indentation cracks reduced the fracture stress to 63 ± 3 MPa for an indentation load of 1 kg and to 35 ± 2 MPa for a 10 kg load (crack aspect ratio of 0.6) aged for 24 h or 30 ± 2 MPa for a 10 kg load (crack aspect ratio of 0.42) aged for 1 week. The practical strength of glass articles is commonly in the range of 30–100 MPa [25] and so the fracture stress of glass indented with even a 10 kg indent is still within the range of practical strength of glass.

The critical stress intensity factor for failure at the tip of an annealed indented glass sample is given by

$$K_{Ic} = Y\sigma\sqrt{\pi c}, \tag{5}$$

Table 3
Mean failure stress and surface crack lengths for indented and annealed samples

Indentation load, P (kg)	Failure stress, σ_f (MPa)	Surface crack length, c (μm)	Experimental geometry factor, Y
0.5	84 ± 2	63 ± 1	0.63 ± 0.02
1.0	69 ± 2	95 ± 2	0.63 ± 0.02
2.0	59 ± 2	148 ± 2	0.59 ± 0.02
3.5	52 ± 1	219 ± 3	0.55 ± 0.01
5.0	48 ± 2	274 ± 10	0.53 ± 0.02
10.0	41 ± 3	443 ± 15	0.49 ± 0.04
10.0†	37 ± 2	420 ± 15	0.56 ± 0.03

Sample marked † aged for 1 week all other samples aged for 24 h.

where, as indicated earlier, $K_{Ic} = 0.75$ MN m$^{-3/2}$, σ is the applied stress at failure and Y is a crack geometry parameter. Eq. (5) was used to determine the crack geometry parameter Y from the measured flaw sizes and the fracture stresses. These experimentally obtained values are given in Table 3.

The critical stress intensity factor for failure at the crack tip of an indented glass sample that has not been annealed is given by

$$K_{Ic} = Y\sigma\sqrt{\pi c} + \frac{\chi_r P}{c^{3/2}}, \quad (6)$$

where the second term accounts for the residual stresses around the indent (see Eq. (4)). The experimentally obtained values of Y and the data in Table 2 were used in Eq. (6) to evaluate χ_r; values of χ_r for different indentation loads are given in Table 4. The relatively large errors are due to the fact that the calculations to obtain χ_r involve taking the difference between two similarly sized numbers. However, it can be seen that, with the exception of the value of χ_r obtained with a load of 0.5 kg, the values are all very similar. The different χ_r obtained with the 0.5 kg load may be connected with the fact that a different indenter was used for this low load. All the values are significantly less than the value of 0.026 reported by Marshall and Lawn [15], which is not surprising as they obtained this value immediately after unloading of the indenter in an inert environment, whereas the 24 h or 1 week aging used here acts to relieve the residual stresses. With the exception of the 0.5 kg load the values are also less than the value of 0.014 reported by Roach and Cooper [16] for soda-lime-silicate glass after aging in air.

Therefore, the initial analysis shows that we have slightly differing parameters for the controlled defects used in the solvent based and water based coatings work. For the solvent based coatings work, the flaw aspect ratio, the a/c value, is 0.6, the geometric factor, Y, is 0.49 ± 0.04 and the residual stress factor, χ_r, is 0.010 ± 0.007. Meanwhile, for the water based coatings work, a/c equals 0.42, Y equals 0.56 ± 0.03 and χ_r equals 0.011 ± 0.005.

4.3. Mechanical testing of coated systems

The mean strengths of the various solvent based coating systems tested are given in Table 5 and the mean strengths of the water based coating systems tested are given in Table 6. The origin of other parameters given in these tables is detailed below. It can be seen that different degrees of strengthening are achieved with both coating systems. In particular, it can be seen that the presence of a silane improves the solvent based coating system with the $S_p/W_{RT}/EH_{sol}$ coating being the most effective. Greater degrees of strengthening are seen with higher coating solution concentrations with the water based coating system.

Fractographic studies of the fracture surfaces showed that failure always started from the tip of the surface crack (point A in Fig. 1(b)). In addition, it has been shown that the solvent based coating system essentially completely filled the

Table 4
Experimentally obtained values of χ_r for the indented glass slides

Indentation load, P (kg)	χ_r
0.5	0.015 ± 0.004
1.0	0.008 ± 0.004
2.0	0.008 ± 0.005
5.0	0.008 ± 0.004
10.0	0.010 ± 0.007
10.0†	0.011 ± 0.005

Sample marked † aged for 1 week all other samples aged for 24 h.

Table 5
Mean failure stresses, equivalent flaw sizes and closure stresses for solvent based coating systems

Coating system	Mean failure stress, σ_f (MPa)	Calculated equivalent flaw size, c_e (μm)	Calculated closure stress, σ_{cl} (MPa)
Uncoated	35 ± 2	458 ± 66	-0.10 ± 0.01
EH_{sol}	68 ± 3	121 ± 17	-33 ± 4
S_p/EH_{sol}	90 ± 5	69 ± 10	-55 ± 7
$S_p/W_{RT}/EH_{sol}$	117 ± 7	41 ± 6	-82 ± 11
$S_p/W_{60}/EH_{sol}$	104 ± 11	52 ± 9	-69 ± 9
EH_{sol}/S	89 ± 11	71 ± 12	-54 ± 7
S	37	410	−2.1

Mean failure stresses based on 6–8 samples.

Table 6
Mean failure stresses, equivalent flaw sizes and closure stresses for partially filled cracks obtained with water based coating systems

Coating	Mean failure stress, σ_f (MPa)	Calculated equivalent flaw size, c_e (μm)	Filled length, $c - c_1$ (Fig. 6) (μm)	Calculated closure stress, σ_{cl} (MPa)
Uncoated	30 ± 1	466 ± 46	0	0.12 ± 0.01
EH_{W_5}	40 ± 8	262 ± 58	24 ± 6	−49 ± 4
$EH_{W_{10}}$	56 ± 10	134 ± 27	42 ± 10	−96 ± 9
$EH_{W_{15}}$	88 ± 10	54 ± 8	150 ± 6	−105 ± 10
$EH_{W_{20}}$	95 ± 15	47 ± 9	204 ± 45	−105 ± 10

Mean failure stresses based on 10 samples.

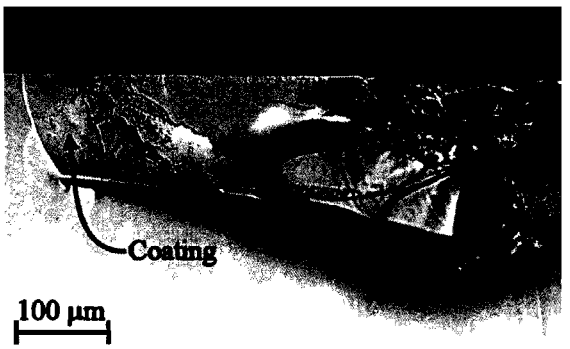

Fig. 4. Typical fracture surface obtained with the $EH_{W_{20}}$ coating system; note the limited extent of coating penetration.

cracks [26]. However the filling with the water based coating system was only partial, with the coating being largely confined to the near crack tip region which can be seen on the left in Fig. 4. The central region of the indent site is on the right in Fig. 4. In the near tip region, Fig. 4 shows that the coating penetrated right to the base of the crack and failed cohesively. There is some evidence of small amounts of coating elsewhere in the crack, particularly just above the lateral crack trace, however, comparison with the other fracture surface (not shown) indicates that the regions where the coating is not visible are not due to adhesive failure.

5. Discussion

Previous work has shown that the adhesion of the coating to the glass as well as coating cohesion is important in determining the efficacy of the coating [26]. In this context good adhesion is believed to arise from chemical bonding of the coating to a substrate. In the following analyses it is therefore assumed, unless otherwise stated, that there is a chemical bond between the coating and the substrate, i.e. good adhesion of the coating to the glass with a high interfacial shear strength is assumed.

5.1. Poisson constraint effect

We have previously suggested that the strengthening effect arises because the coating in the crack is only present in a very thin layer and thus, because of Poisson ratio effects, it behaves mechanically as if it had properties similar to the bulk glass [4]. An estimate of the effective modulus of the layer may be made by considering the coating in the crack as a thin layer between two rigid substrates (see Fig. 5). If the layer is very thin and the interfacial shear strength is sufficiently high, the application of a stress as shown in Fig. 5 will lead to very limited lateral strains in the coating. In the limit of completely rigid substrates,

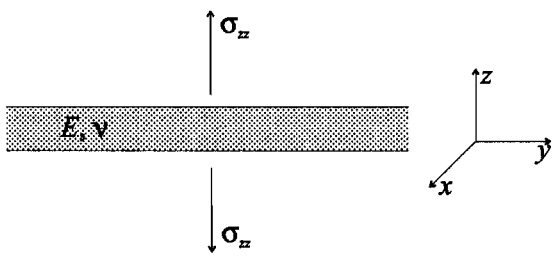

where
E = Young's modulus of coating
ν = Poisson's ratio of coating
σ_{zz} = applied stress

Fig. 5. Geometry used in analysing Poisson constraint effect.

the lateral shear strains will be equal to zero i.e. $\varepsilon_{xx} = \varepsilon_{yy} = 0$. In this case the volume expansion, e, becomes

$$e = \varepsilon_{xx} + \varepsilon_{yy} + \varepsilon_{zz} = \varepsilon_{zz}. \tag{7}$$

The stress in the layer is given by [27]

$$\sigma_{zz} = \frac{vE}{(1+v)(1-2v)}e + \frac{E}{1+v}\varepsilon_{zz}, \tag{8}$$

where E and v are the Young's modulus and the Poisson's ratio of the layer. Therefore, substituting Eq. (7) into Eq. (8) and rearranging, we obtain an effective modulus for the layer given by

$$E_{\text{eff}} = \frac{\sigma_{zz}}{\varepsilon_{zz}} = \frac{1-v}{(1+v)(1-2v)}E. \tag{9}$$

For an epoxy resin with Poisson's ratio of 0.4 and a Young's modulus of ~3 GPa [28], this gives an effective modulus of ~6.4 GPa, which is significantly less than that of the glass. The effective modulus would only start to approach that of glass if v started to approach 0.5. This would suggest that a rubbery layer should have a high effective modulus. However, in practice the Young's modulus of a rubbery material is much lower (~1 MPa for S coatings [28]) and the resultant effective modulus is therefore low. Hence, the S coatings provide little or no strengthening (see Table 5).

5.2. Crack shortening

Fabes and co-workers [1,2] suggested that the coatings partially heal and thereby shorten the flaws. If a crack is filled by a material that responds in the same way as the bulk material when a load is applied, it is reasonable to assume that the flaw is healed by this material. As Fabes and co-workers were using sol–gel derived silica coatings, produced via heat-treatments at temperatures up to 1000 °C, such an assumption is reasonable. Given the Poisson's ratio calculations, outlined in the previous section, it is questionable whether epoxy coatings can respond in the same way as the bulk material.

However, assuming that the coatings do impart a degree of crack healing, we can calculate an equivalent flaw size for the strengthened samples and attempt to relate it to features on the fracture surface. There are two major possibilities: (1) the widest parts of the crack are not filled so that the crack is effectively shortened but has a similar shape to the original flaw and (2) as suggested by Fabes and co-workers [1,2] the coating does not reach the tip of the crack so that the flaw becomes effectively an embedded flaw with a different shape from the original crack.

For the first case we assume that the flaw both before and after filling has the same geometry. Hence an equivalent flaw size, c_e, may be calculated using

$$K_{\text{Ic}} = Y\sigma_f\sqrt{\pi c_e} + \frac{\chi_r P}{c^{3/2}}. \tag{10}$$

The residual stress term in Eq. (10) (second term on the right hand side) is related to the original flaw size, c, rather than the equivalent flaw size, c_e, because flaw filling does not relieve residual stresses arising from indentation. The equivalent flaw sizes calculated using Eq. (10) are given in Tables 5 and 6. As one would expect, the flaw size decreases with increasing strength. However, as noted above, with the solvent based coatings, fractographic evidence has shown that the entire crack is essentially filled by the coating which means that the calculated equivalent flaw sizes cannot be related to any features on the fracture surfaces. With the water based coatings, fractography shows that essentially only the end region of the crack is filled, and thus, it would seem reasonable that the equivalent flaw size should be related to the size of the unfilled region. However, all the calculated equivalent flaw sizes are significantly less than the size of the unfilled region (e.g. for the $EH_{W_{10}}$ coating the size of the unfilled region is 425 ± 21 μm compared to an equivalent flaw size of 134 ± 27 μm) which indicates that simple crack shortening does not explain the increase in strength.

The alternative approach due to Fabes and co-workers [1,2] assumes that the coating does not reach all the way to the crack tip, and thus, there is an 'embedded' flaw with a different geometry from the original flaw that is responsible for failure. Fabes and co-workers give stress intensity factors for failure both from the original crack tip and

from the deepest point to which the resin penetrates. They concluded that, in their system, failure did not occur from the original crack tip. However, with the coating systems studied here, fractographic studies have shown both that the resin penetrates to the ends of the open crack and that failure always occurs from the site where the original open crack intercepts the sample surface.

Therefore, flaw shortening would appear not to explain the strengthening of glass by epoxy coatings. This is because firstly such coatings do not behave as if they have similar properties to the bulk glass, even when they are confined within a crack, and secondly the calculated equivalent flaw sizes cannot be related to either the observed degree of crack filling or to the locus of failure.

5.3. Thermal stresses

Wang and James [3] suggested that thermal expansion mismatch stresses between a coating and the glass substrate would lead to stresses in the surface coating layer that could explain the strengthening effect of coatings. For the low expansion coefficient coating system that they developed, they were able to show that this mechanism was plausible. However Chen et al. [29] have previously shown that, for the solvent based coatings studied here, tensile rather than compressive stresses are generated within the coating. The stresses in the coating are given by

$$\sigma = \frac{E_{rg}}{1 - \nu_{rg}} (\alpha_{rg} - \alpha_g) \Delta T, \tag{11}$$

where E_{rg}, ν_{rg} and α_{rg} are the 'glassy' Young's modulus, Poisson's ratio and thermal expansion coefficient of the resin, α_g is the thermal expansion coefficient of the glass, and ΔT is the difference in temperature between the curing temperature and room temperature; this makes the reasonable assumption that the glass transition temperature of the coating is approximately equal to the curing temperature. To obtain the balancing compressive stress in the glass, we assume that the stresses in both the coating (which coats both sides of the glass) and the substrate are uniformly distributed, in which case the stress in the substrate is given by

$$\sigma = -\frac{E_{rg}}{1 - \nu_{rg}} \frac{2t_c}{t_g} (\alpha_{rg} - \alpha_g) \Delta T, \tag{12}$$

where t_c and t_g are the thickness of the coating and the glass, respectively. For the solvent based coatings, taking the thermal expansion coefficient of the glass to be 9×10^{-6} °C^{-1} and that of the resin to be 150×10^{-6} °C^{-1} [29], and noting that the system was (post-)cured at 100 °C, the coating thickness was ~3 μm and the glass thickness was 1.2–1.5 mm, the tensile stress in the coating is ~56 MPa and the compressive stress in the glass is ~0.2 MPa. With the water based system, assuming the same coating properties but noting that the coating was cured at 220 °C and was ~10 μm thick, with a glass thickness of 1.1 mm, the tensile stress in the coating is ~140 MPa and the compressive stress in the glass is ~2.5 MPa. In both cases, the compressive stresses in the glass are clearly insufficient to explain the strengthening effect that arises from epoxy based coating systems.

5.4. Closure stresses

Roach et al. [9] have suggested that, when material completely fills and thereby bridges a crack, this material exerts a closure stress, σ_{cl}, which retards crack propagation when the crack is subjected to a tensile force. This stress is assumed to be uniformly distributed over the whole crack. In this case, the stress intensity factor at failure in coated glass must be given by

$$K_{Ic} = Y\sigma_f\sqrt{\pi c} + \frac{\chi_r P}{c^{3/2}} + K_{cl}, \tag{13}$$

where K_{cl} is the stress intensity factor due to the restraint or closure stress produced by the coating.

With the solvent based coating system, the cracks are completely filled by the coating. Thus, assuming that complete filling leads to a uniformly distributed closure stress over the crack walls, and that the same geometric factor can be used as for the applied bending stress, we have

$$K_{Ic} = 0.49\sigma_f\sqrt{\pi c} + \frac{0.9810 \times 10^{-6}}{c^{3/2}} + 0.49\sigma_{cl}\sqrt{\pi c}, \tag{14}$$

where σ_{cl} is the closure stress in MPa. The fracture stress, σ_f, is also in MPa, the fracture toughness, K_{Ic} is in $MN\,m^{-3/2}$ and the crack length, c, is in metres. The closure stresses evaluated using Eq. (14) are given in Table 5. The negative sign indicates that the closure stresses are compressive, which is necessary if they are actually going to act to close the crack. The closure stress for the uncoated system is essentially zero as expected. As can be seen by a simple rearrangement of Eq. (14), the closure stress is linearly related to the mean failure stress, and thus, the largest closure stress was obtained with the $S_p/W_{RT}/EH_{sol}$ system, which we have previously demonstrated gives the best strengthening results.

With the water based epoxy system, crack filling is only partial, with the coating essentially being confined to a region near the end of the cracks. The degree of filling, expressed as filled length from the crack tip, depends on the concentration of the coating solution (see Table 6). Given that failure always starts at the crack tip, an estimate of the closure stress may be made using a centre cracked plate model. As shown in Fig. 6, it is assumed that partial filling of the centre cracked plate leads to uniform closure stresses being distributed over the partially filled region. In this case the closure stress intensity factor is given by

$$K_{cl} = 2Y'\sigma_{cl}\left(\frac{c}{\pi}\right)^{1/2}\int_{c_1}^{c}\frac{\sigma dx}{\sqrt{c^2-x^2}}, \tag{15}$$

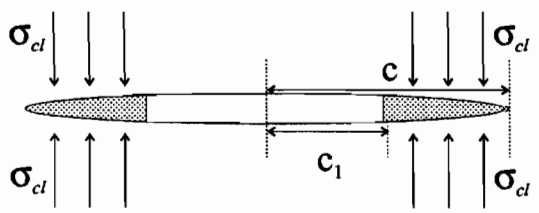

where
c = crack length
c_1 = unfilled crack length
σ_{cl} = closure stress

Fig. 6. Geometry used in calculating closure stresses in the case of a partially filled crack.

where Y' is a geometric constant that accounts for the finite width of the plate (see, for example, [30]). Integrating Eq. (15) gives

$$K_{cl} = 2Y'\sigma_{cl}\left(\frac{c}{\pi}\right)^{1/2}\left[\frac{\pi}{2} - \sin^{-1}\frac{c_1}{c}\right]. \tag{16}$$

A difficulty arises here because the value of Y' is unknown. However, again we assume that the same geometric factor as that used for the applied bending stresses can be used (0.56 ± 0.03 in this case), which gives

$$K_{Ic} = 0.56\sigma\sqrt{\pi c} + \frac{1.0791\times10^{-6}}{c^{3/2}} + 2\times0.56\sigma_{cl}\left(\frac{c}{\pi}\right)^{1/2}\left[\frac{\pi}{2} - \sin^{-1}\frac{c_1}{c}\right]. \tag{17}$$

Once again, the closure stress, σ_{cl}, and the fracture stress, σ_f, are in MPa; the fracture toughness K_{Ic} is in $MN\,m^{-3/2}$ and both the crack length, c, and the unfilled crack length, c_1 are in metres. Values of closure stress calculated in this fashion are given in Table 6. It can be seen that the calculated closure stresses are similar for all but the most dilute coating solution (EH_{W_5}) which suggests that, above a certain minimum value, the concentration of the coating solution only really effects the amount of crack filling, and has little further effect on the mechanical properties of the resultant coating.

An obvious question concerns the origin of such closure stresses. As the resin is cured at temperatures of 100 or 220 °C one possibility is thermal expansion mismatch stresses between the resin and the glass generated within the crack rather than those generated on the sample surface, which were discussed above (Section 5.3). Consider a region of the coating in a crack as shown in Fig. 7. On cooling from the cure temperature, the resin in the crack will not be able to contract as much as if it were unconstrained because $E_{glass} \gg E_{resin}$. This gives rise to a strain in the resin given by

$$\varepsilon_{resin} = \frac{w_0^{crack} - w_0^{resin}}{w_0^{resin}}, \tag{18}$$

where w_0^{crack} and w_0^{resin} are the widths of a given segment of the crack and the unconstrained resin at room temperature. w_0^{resin} is related to the width

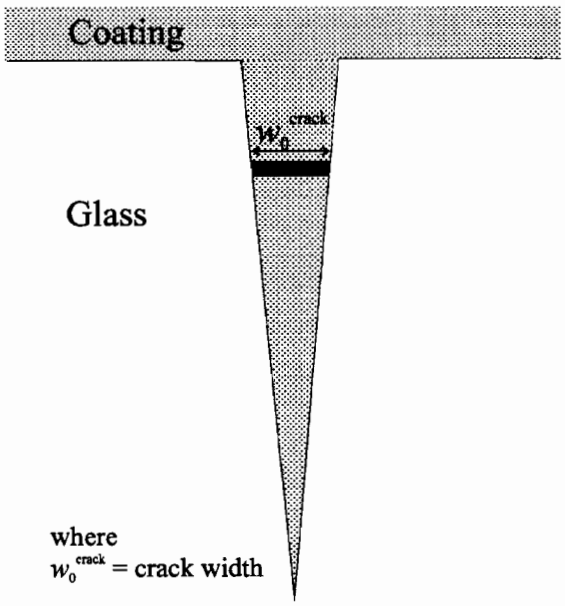

Fig. 7. Geometry used in analysing thermal expansion mismatch stresses within the crack.

of the same segment of crack at the curing temperature, w_C^{crack}, by

$$w_0^{resin} = w_C^{crack}(1 - \alpha_{rg}\Delta T), \tag{19}$$

where α_{rg} is the glassy thermal expansion coefficient of the resin and ΔT is the difference in temperature between the curing temperature and room temperature. But w_C^{crack} is given by

$$w_C^{crack} = w_0^{crack}(1 + \alpha_g \Delta T), \tag{20}$$

where α_g is the thermal expansion coefficient of the glass. Hence the strain in the resin is given by

$$\varepsilon_{resin} = \frac{1}{(1 + \alpha_g \Delta T)(1 - \alpha_{rg}\Delta T)} - 1. \tag{21}$$

Unfortunately the thermal expansion coefficient of the resin is not a well characterised quantity for the various coating systems studied, and thus, only a rough estimate of the strains in the coatings studied can be obtained.

For the solvent based coatings, taking the coating properties as above (Sections 5.1 and 5.3), gives $\varepsilon_{resin} = 0.011$ and a closure stress of ~34 MPa. This value is very similar to the calculated closure stress for the EH_{sol} system although it is lower than the values for the more effective coating systems (see Table 5). This suggests that, although thermal stresses may be the origin of the closure stresses, because of the interlayers that are present when a silane is present (especially in the primed system), the analysis is over-simplified for the silane containing coating systems.

The same calculation can be carried out for the case where just the silane was applied. In this case, the coating was cured at 60 °C and we take the thermal expansion coefficient of the silane coating to be 3×10^{-4} °C^{-1} [28]. Thus, $\varepsilon_{silane} = 0.012$, and using the modulus given above (Section 5.1), the closure stress is ~0.012 MPa which is significantly smaller than the calculated value given in Table 5. However, both values indicate that the strengthening effect is negligible.

For the water based coating systems, again taking the coating properties as detailed above (see Sections 5.1 and 5.3), and noting that in this case the coating was cured at 220 °C, $\varepsilon_{resin} = 0.029$ and the closure stress is 87 MPa. This value is similar albeit a bit lower than the calculated values for all the water based coatings examined apart from coating $EH_{W_{10}}$. This suggests that crack closure arising from thermally induced strains in those regions of the crack bridged by the coating are indeed responsible for the observed strengthening effects.

Given the approximate nature of these calculations, the agreement between the calculated thermal expansion mismatch stresses within the crack and the calculated closure stresses strongly suggests that it is thermal expansion mismatch stresses within the crack, rather than in the surface layers, that give rise to the observed strengthening effect.

6. Conclusions

The strengthening of glass by epoxy based coatings depends on penetration of pre-existing defects in the glass surface. However an increased effective modulus due to Poisson's ratio effects or crack shortening due to coating penetration do not explain why the coatings are effective. Instead we have shown that closure stresses generated by

thermal expansion mismatch stresses within the flaws, not in coating surface layer, are a plausible explanation for the observed degree of strengthening. Therefore to strengthen glass, epoxy based coatings must penetrate the flaws; this may be problematic with some naturally occurring defects [31]. The actual coating on the surface is thought to be less important except that sufficient coating penetration is unlikely to occur unless the coatings are laid down on the surface.

Acknowledgements

We thank the Engineering and Physical Sciences Research Council, Swindon, UK and Pilkington plc, St. Helens, UK for providing financial support for B.R.W. and the University of Sheffield, UK for providing financial support for F.H.W.

References

[1] B.D. Fabes, D.R. Uhlmann, J. Am. Ceram. Soc. 73 (1990) 978.
[2] B.D. Fabes, G.D. Berry, J. Non-Cryst. Solids 121 (1990) 357.
[3] T.H. Wang, P.F. James, J. Mater. Sci. 26 (1991) 354.
[4] F.H. Wang, R.J. Hand, B. Ellis, A.B. Seddon, Phys. Chem. Glasses 36 (1995) 201.
[5] F.H. Wang, X.M. Chen, R.J. Hand, B. Ellis, A.B. Seddon, Br. Ceram. Proc. 54 (1995) 119.
[6] F.H. Wang, X.M. Chen, B. Ellis, R.J. Hand, A.B. Seddon, Mater. Sci. Technol. 13 (1997) 163.
[7] B.R. Whittle, J.D. Whittle, R.J. Hand, B. Ellis, R.D. Short, J. Adhes. 77 (2001) 1.
[8] V. Verganelakis, P.D. Nicolaou, G. Kordas, Glass Technol. 41 (2000) 22.
[9] D.H. Roach, S. Lathabai, B.R. Lawn, J. Am. Ceram. Soc. 71 (1988) 97.
[10] R.J. Hand, F.H. Wang, B. Ellis, A.B. Seddon, Phys. Chem. Glasses 39 (1998) 305.
[11] T.-H. Cheng, F.R. Jones, D. Wang, Compos. Sci. Technol. 48 (1993) 89.
[12] R.J. Hand, F.H. Wang, B. Ellis, A.B. Seddon, J. Sol–Gel Sci. Technol. 13 (1998) 695.
[13] B.R. Lawn, E.R. Fuller, J. Mater. Sci. 10 (1975) 2016.
[14] D.B. Marshall, J. Am. Ceram. Soc. 66 (1983) 127.
[15] D.B. Marshall, B.R. Lawn, J. Mater. Sci. 14 (1979) 2001.
[16] D.H. Roach, A.R. Cooper, J. Am. Ceram. Soc. 68 (1985) 632.
[17] S.M. Smith, R.O. Scattergood, J. Am. Ceram. Soc. 75 (1992) 305.
[18] V.M. Sglavo, D.J. Green, Acta Metall. Mater. 43 (1995) 965.
[19] C.B. Ponton, R.D. Rawlings, Mater. Sci. Technol. 5 (1989) 865.
[20] S.M. Wiederhorn, J. Am. Ceram. Soc. 52 (1969) 99.
[21] R.H. Marion, in: S.W. Freiman (Ed.), Fracture Mechanics Applied to Brittle Materials ASTM STP678, American Society for Testing and Materials, 1979, p. 103.
[22] J.R. Varner, in: C.R. Kurkjian (Ed.), Strength of Inorganic Glass, Plenum Press, New York, 1975, p. 389.
[23] B.R. Whittle, R.J. Hand, J. Am. Ceram. Soc. 84 (2001) 2361.
[24] D.B. Marshall, B.R. Lawn, A.G. Evans, J. Am. Ceram. Soc. 65 (1982) 561.
[25] B.R. Lawn, A.G. Evans, J. Mater. Sci. 12 (1977) 2195.
[26] R.J. Hand, F.H. Wang, B. Ellis, A.B. Seddon, in: M.W. Brown, E.R. de los Rios, K.J. Miller (Eds.), Fracture from Defects, vol. I, EMAS, Cradley Heath, 1998, p. 557.
[27] S. Timoshenko, J.N. Goodier, in: Theory of Elasticity, 2nd Ed., McGraw-Hill, New York, 1951, p. 8.
[28] B. Ellis (Ed.), Polymers: A Property Database CD-ROM Version 6.0.2, CRC, 2000.
[29] X.M. Chen, B. Ellis, F.H. Wang, A.B. Seddon, J. Non-Cryst. Solids 185 (1995) 1.
[30] H.L. Ewalds, R.J.H. Wanhill, in: Fracture Mechanics, Edward Arnold, London, 1991, p. 40.
[31] J.G.R. Kingston, R.J. Hand, Phys. Chem. Glasses 41 (2000) 1.